10-22-1999

# FiberGLAST: a scintillating fiber approach to the GLAST mission

Geoffrey N. Pendleton
*University of Alabama - Huntsville*

W Robert Binns
*University of Alabama - Huntsville*

Martin W. Israel
*Washington University in St Louis*

P L. Hink
*Washington University in St Louis*

M L. Cherry
*Louisiana State University - Baton Rouge*

***See next page for additional authors***



## Recommended Citation

Geoffrey N. Pendleton ; W. Robert Binns ; Martin H. Israel ; Paul L. Hink ; Michael L. Cherry ; William S. Paciesas ; Richard M. Kippen ; Robert S. Mallozzi ; Thomas A. Parnell ; Gerald J. Fishman ; Tumay O. Tumer ; Mark J. Christl ; Robert B. Wilson ; James H. Buckley ; Georgia A. Richardson ; Surasak Phengchamnan ; Keith R. Rielage ; Gerald Karr ; Donald B. Wallace ; James M. Ryan ; Mark L. McConnell and John R. Macri "FiberGLAST: a scintillating fiber approach to the GLAST mission", Proc. SPIE 3765, EUV, X-Ray, and Gamma-Ray Instrumentation for Astronomy X, 12 (October 22, 1999); doi:10.1117/12.366500; http://dx.doi.org/10.1117/12.366500

**Authors**
Geoffrey N. Pendleton, W Robert Binns, Martin W. Israel, P L. Hink, M L. Cherry, W Paciesas, R M. Kippen, Robert S. Mallozzi, Thomas A. Parnell, Gerald J. Fishman, O T. Tumer, Mark J. Christl, Robert B. Wilson, J Buckley, Georgia A. Richardson, Surasak Phengchamnan, Keith R. Rielage, Gerald Karr, Donald B. Wallace, James M. Ryan, Mark L. McConnell, and John R. Macri

# FiberGLAST: a scintillating fiber approach to the GLAST mission

G.N. Pendleton[a], W.R. Binns[b], M. H. Israel[b], P. L. Hink[b], M.L.. Cherry[e], W. S. Paciesas[a], R. M Kippen[a], R.S. Mallozzi[a], T. A. Parnell[a], G.J. Fishman[c], T. O. Tumer[d], M. J. Christl[c], R. B. Wilson[c], J. H. Buckley[b], G. Richardson[a], S. Phengshamnan[a] , K. Rielage[b], G. Karr[a], D. Wallace[a], J.M. Ryan[f], M. L. McConnell[f], J.R Macri[f]

[a] Dept. of Physics, University of Alabama in Huntsville
[b] Dept. of Physics, Washington University in St. Louis
[c] Marshall Space Flight Center
[d] University of California Riverside
[e] Louisiana State University
[f] University of New Hampshire

## ABSTRACT

FiberGLAST is a scintillating fiber gamma-ray detector designed for the GLAST mission. The system described below provides superior effective area and field of view for modest cost and risk. An overview of the FiberGLAST instrument is presented, as well as a more detailed description of the principle elements of the primary detector volume. The triggering and readout electronics are described, and Monte Carlo Simulations of the instrument performance are presented.

## 1. INTRODUCTION

The FiberGLAST instrument is a wide field-of-view, high effective area gamma-ray pair telescope designed for an all-sky survey of BLAZARs, Gamma-Ray Bursts, and other high-energy astrophysical phenomena. The performance of FiberGLAST is optimized for the measurement of a large population of rapidly changing high-energy transients. The large field of view provides superior continuous monitoring of isotropically distributed variable sources. The large effective area permits more precise spectral characterization over short time intervals. This instrument takes advantage of recent advances in plastic scintillating fibers and their readout systems. This advanced technology allows us to develop an instrument design optimized to measure the most interesting properties of the high-energy phenomena to be studied.

## 2. INSTRUMENT DESCRIPTION

The FiberGLAST instrument is designed to maximize effective area and field of view[1]. A diagram of the overall instrument is shown in Figure 1. The lighter central region is the tracker section. It is comprised of ~90 fiber detector planes with 1/50'th r.l. thick converter plates in each plane. This part of the system measures direction and performs calorimetry for lower energy photons, and measures the direction and provides reduced calorimetric information for higher energy photons. Directly beneath it, represented by the darker region, is the calorimeter section that provides enhanced calorimetric information for higher energy photons. It contains ~30 detector planes with 1/6'th r.l. thick converter plates in each plane. These two sections together are referred to as the detector stack. The readout system and trigger electronics are distributed around the sides of the detector stack, shown in this diagram as planes of small cubes. The instrument is supported by an aluminum frame to which the anti-coincidence system is also attached. The anti-coincidence system is comprised of two orthogonal layers of scintillating boards . The entire instrument has four support contact points though which it is attached to the spacecraft.

### 2.1 Detector Stack Hardware

The detector planes for both the tracker and calorimeter are simple components. Each detector plane has a converter plate of high-Z material on top that stimulates pair production of high energy photons and bremsstrahlung of high energy electrons. Directly underneath this plate are two closely packed orthogonal layers of scintillating fibers used to detect the



Part of the SPIE Conference on EUV, X-Ray, and Gamma-Ray Instrumentation for Astronomy X
Denver, Colorado • July 1999 SPIE Vol. 3765 • 0277-786X/99/$10.00

passage of minimum ionizing particles. Plastic honeycomb fills the rest of the space between each layer of fibers so that the detector planes are fully supported over their entire area.

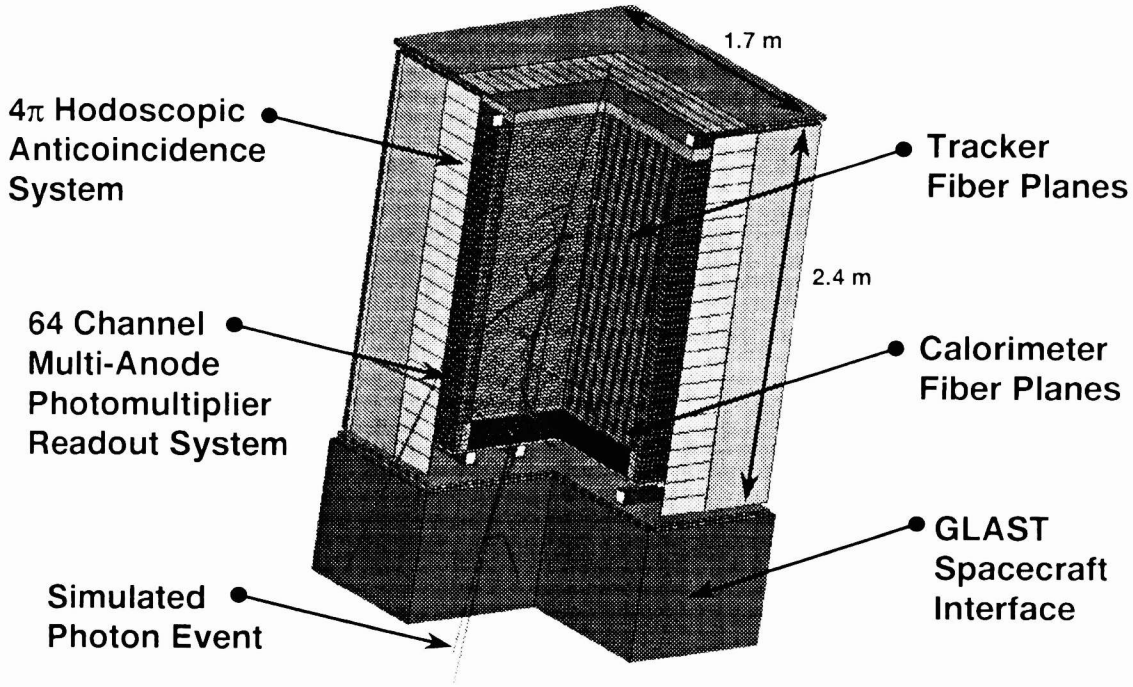


**Figure 1 Diagram of FiberGLAST Instrument**

The primary component of the fiber readout system is the R5900-00-064 multi –anode photo-multiplier tube (MAPMT). These MAPMTs have 64 bi-alkali photocathodes and an 8x8 anode array of 2 mm square pixels. They have a quantum efficiency of 22-25%, a dark count of typically ~5/anode/second, a very low cross-talk between anodes (<2%), and are low power (4 mW/tube using a 200M bleeder string).

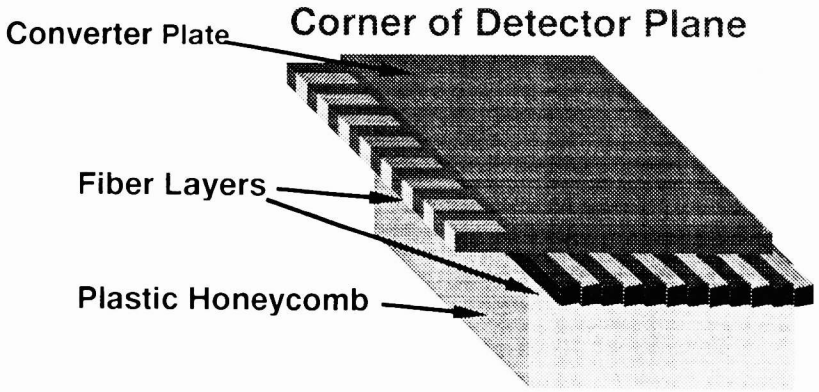


**Figure 2**

The tube response is very fast, with an anode pulse rise time of 1.5 n.s. They are quite compact with dimensions 28mm x 28mm x 33mm. We have also performed a shake test at MSFC on the MAPMT to determine whether it can survive the launch environment for a space-based experiment. Two tubes were subjected to random vibration testing at levels slightly exceeding Delta II qualification levels. No damage or degradation occurred as a result of this test. A single anode version of

this tube has previously flown on the AMS experiment launched on the Space Shuttle. It thus appears that this tube can survive the launch environment and is suitable for use in space.

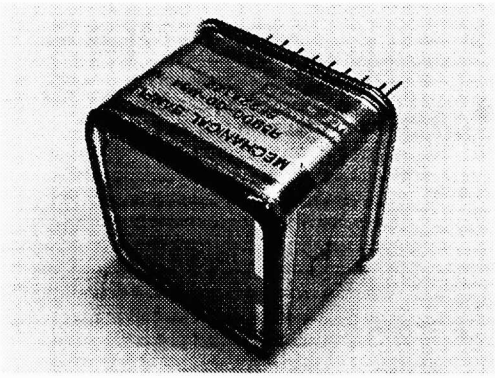

**Figure 3: R5900-00-064 multi –anode photo-multiplier tube**

In the tracker each fiber is read out by a single anode , and each anode is read out by a self triggering channel of an ASIC. The MAPMTs are grouped together physically and electronically into a group of six contiguous tubes mounted on the front end electronics board (FEE). The FEE boards also distribute the high and low voltage power, and communicate the fiber data and trigger signals to the trigger electronics. The fibers are mounted through a cookie to the readout group of tubes on the FEE board. The ASICs are daisy chained together so that trigger logic can be applied to this group of channels.

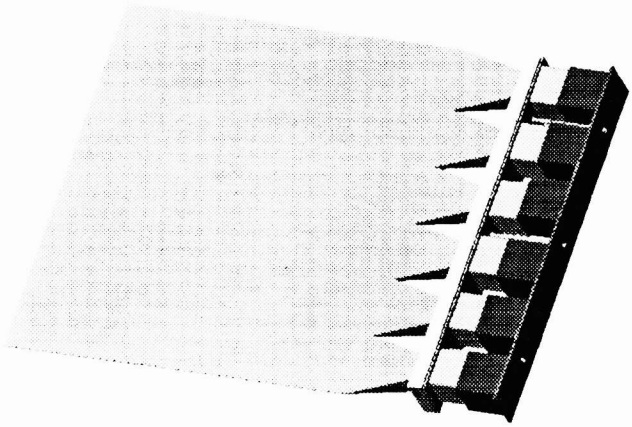

**Figure 4: Fiber Group**

### 2.2 Trigger Electronics and Logic

The trigger and background rejection concepts are illustrated in figure 5. The fiber groups on fiberGLAST are distributed Equally on four sides of the fiber stack volume ($-x$, $+x$, $-y$, and $+y$ sides). To avoid having to communicate large amounts of data from one side to the other, our concept begins with a low-level (*level-0*) trigger that operates "locally" (i.e., independently) on each side. This analog/digital logic system must quickly (~1 μs) trigger whenever any particle track substantially longer than might be expected due to noise interacts anywhere in the fiber stack. The system must then reduce the potentially large amount of fiber readout data into a small set of parameters (referred to as *topology parameters*) that can be used for distinguishing source and background events in later processing levels.

Combining trigger topology data from all four sides of the fiber stack forms a more robust set of parameters that yields a rough indication of the major axis of the event, its depth and its width. This small amount of data in each of the two orthogonal fiber directions is then combined with the addresses of triggered anti-coincidence panels to reject probable background events (*level-1 background reject*). If the event is accepted, a signal is sent to acquire the addresses of individual fibers from front-end storage buffers-otherwise, the level-0 trigger is reset and new events can trigger.

**Figure 5: Diagram of trigger logic**

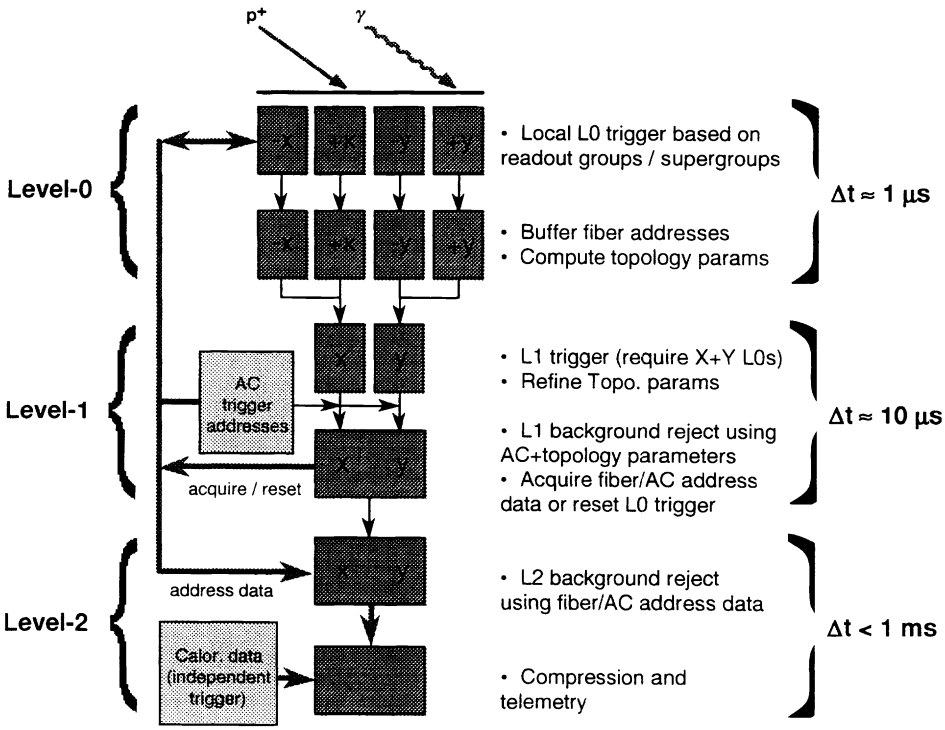


Our simulation results indicate that this general concept is capable of providing good source-to-background filtering (~95% rejection of cosmic-ray proton triggers). For further background rejection (e.g., rejection of Earth albedo gamma rays) the addresses of the individual fiber hits are required. The Level-2 background rejection concept uses the fiber hit data to distinguish and reject much of the background remaining after level-1. This phase of processing also uses the fiber address data to compute a rough direction for gamma-ray events, and accept/reject them based on the position of the earth at the time. Fiber and anti-coincidence address data for the remaining events are then packaged for telemetry to the ground.

To realize a fast, low-level trigger the many individual fiber readout elements are combined into larger entities called readout *groups*. The function of a readout group is to combine data from any of its constituent fiber readout channels (via ASICs coupled to MAMPTs) to form a group-level trigger signal. In the baseline design there are 5 readout groups per fiber layer in both the *x* and *y* dimensions. The amount of segmentation is a trade between several competing factors, including the total number of trigger channels, the spatial resolution of the trigger. This particular segmentation scheme was chosen to yield reasonable spatial resolution for level-1 background rejection, while keeping the number of trigger channels manageable. The readout devices for alternating fiber layers are located on opposite sides of the fiber stack, so having 5 readout groups per layer results in 5×45=225 readout groups on each of the four sides of the stack. A readout group is realized in hardware by a front-end-electronics (FEE) circuit board that combines the ASIC outputs from 6 MAPMTs to form a fast trigger signal and provides fast data buffers to temporarily store fiber address data. The FEE readout group hardware also provides serial data lines to transmit the addresses (and pulse heights in the calorimeter) of individual fiber hits upon receiving a Level-1 acquire signal. Due to random noise in the fiber readout devices, it is not sufficient to trigger the entire data readout system based on a trigger signal from a single readout group. Rather, we need a system that only triggers on real particle tracks whose most characteristic feature is that they span several consecutive planes in the fiber stack. Our trigger system concept uses this feature by combining several groups together in a logical entity called a *supergroup*. It is the combined group signals in a supergroup that actually trigger the data processing chain. The size, geometry and logic for a

supergroup trigger affect the background rejection efficiency, gamma-ray energy range and gamma-ray field-of-view of the instrument. In our baseline system, a trigger supergroup is defined to yield good gamma-ray efficiency >15 MeV up to ~80 deg off-axis. It is a rectangle 2 groups wide and 4 groups high, with a level-0 trigger condition requiring group triggers on 3 or more of the four layers. In order to enhance the detection efficiency for low-energy gamma rays, the supergroups are overlapping vertically by every two groups. The overlapping supergroup concept also gives the system a great deal of redundancy. In the horizontal direction, there are 10 supergroups around the perimeter. These 10 horizontal supergroups do not overlap, but they are staggered so events that don't trigger on one side of the stack can independently trigger on the opposite side.

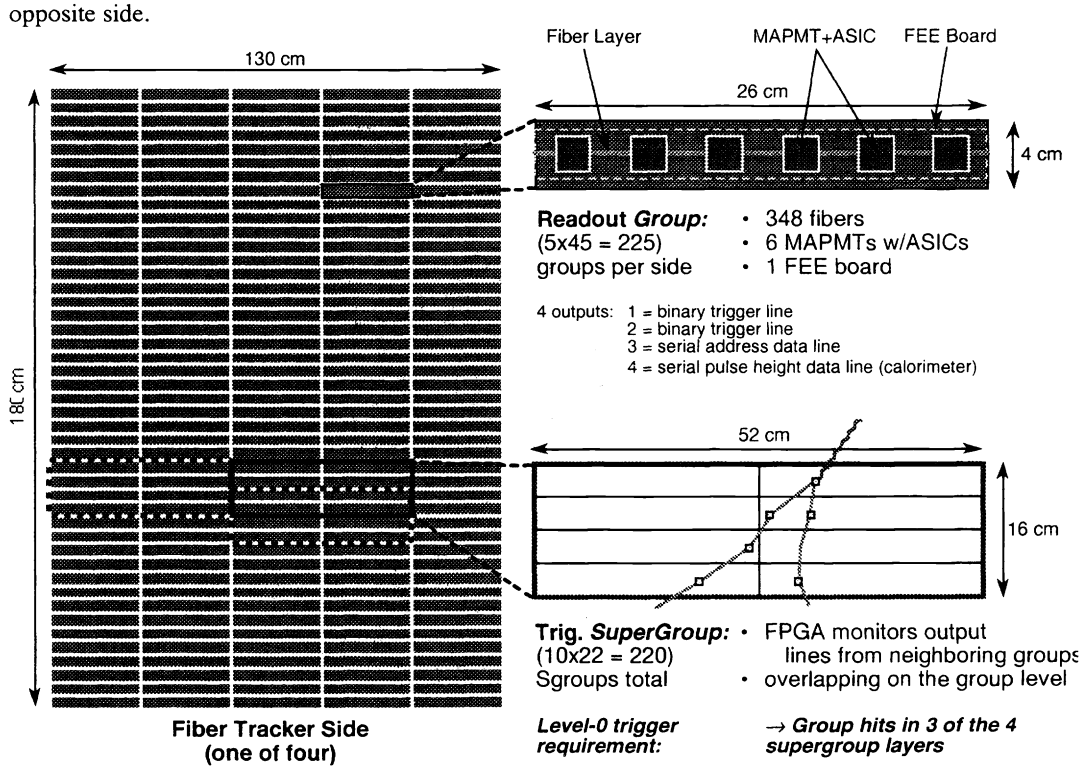


**Figure 6: Diagram of Group and Supergroup Concepts**

In hardware, the supergroup concept is realized by having logic devices such as field-programmable gate arrays (FPGAs) monitoring the outputs of several readout groups, simultaneously. The FPGA configuration design is a trade between having a few large devices that form many supergroups and many smaller devices that form fewer supergroups. The advantage of the latter is greater redundancy in the case of failure. The exact configuration will also depend on power requirements and is a topic for the development study.

When one or more supergroup triggers occur on one side of the stack, the level-0 hardware (FPGAs) begins to reduce the group-level data. The idea is to compute a small number of *topology parameters* that sufficiently identify the shape and direction of the particle track for background rejection purposes. In our baseline concept, the topology parameters consist of simple data such as the highest, lowest, leftmost and rightmost trigger group. While somewhat more elaborate concepts have been investigated, the amount of topology parameter data is expected to be small (<12 numbers per side), allowing fast communication with the level-1 background rejection system. All other data (i.e., individual fiber addresses) are stored in FEE/ASIC buffers until a level-1 acquire signal is received. The final task of the level-1 system is to communicate its accept/reject decision to the front-end electronics of both the tracker and calorimeter. This is naturally performed through the FPGAs that comprise the level-0 trigger hardware. When an event is rejected, a reset signal propagates to all the FEE/ASICs, and the level-0 trigger system is ready for new events. When an event is accepted, the FEE/ASIC buffers that have been storing fiber addresses are emptied into secondary buffers before resetting the system. The fiber addresses are then transmitted via a serial data bus to the level-2 processor.

The level-1 system described above can quickly remove many background events before full readout of the fiber data because it minimizes the amount of information being transmitted large distances and uses simple processing logic.

However, the rate of remaining background events is too high to meet the spacecraft telemetry requirement. A second level of background rejection is therefore needed. This level-2 system has the benefit of being able to use the full fiber resolution to screen the background events. The system based on the use of a programmable digital signal processor (DSP) and a large multi-event memory buffer.

## 3. PERFORMANCE SIMULATIONS

### 3.1 Monte Carlo Simulations Package

Using the particle transport and detector-building tools of GEANT, we have developed a simulation software package called SIFSIM (ScIntillating Fiber SIMulation) that includes the essential elements required to study the performance of *FiberGLAST*. SIFSIM uses the particle transport routines of GEANT to propagate user-selected particle distributions through detailed mass models of various *FiberGLAST* configurations. In the case of hadrons, the GEANT-FLUKA[2] interface is used to generate the interactions. The choices for incident particle distributions include beams for simulating nearby calibration sources, astrophysical "point" sources, extended diffuse sources and various background distributions—all with the choice of several different particle energy spectra. Energy deposited in the active detector elements is accumulated throughout the simulation process until all primary and secondary particles have either escaped the system or dropped below a kinetic energy threshold of 10 keV. The cumulative energy deposits are recorded in event list files for later analysis.

### 3.2 Event Reconstruction Algorithms

The tracker algorithm in this analysis package actually calculates all the observables necessary for photon response function determination. Both the directional and calorimetric observables are calculated by this algorithm. The first algorithm, moments analysis, calculates information necessary to perform some crude calorimetric analysis and to determine the approximate direction of the photon as well as to identify which end of the photon shower has the pair conversion vertex.

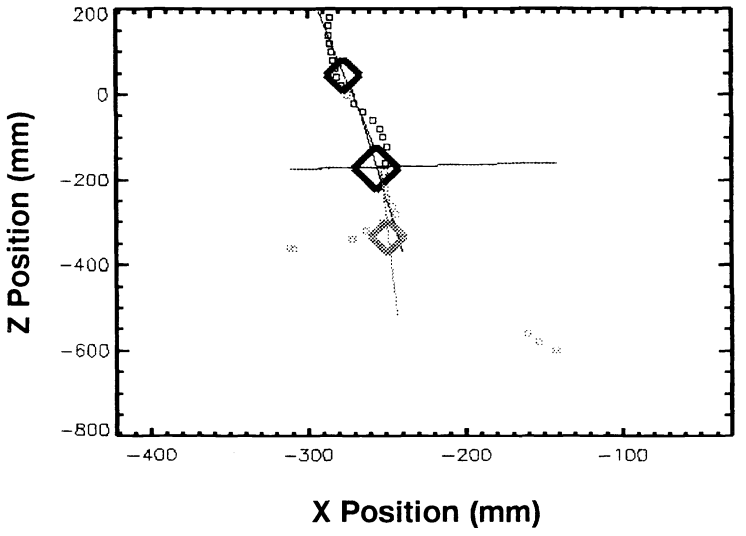


**Figure 7: Diagram of moments analysis**

The unprocessed photon event data from one side of FiberGLAST ( i.e. the X-Z side of the instrument, for example), consists in the tracker of the addresses of fiber hits above threshold, and in the calorimeter of the fiber hit addresses and an energy deposition measurement for each fiber. The first step in the moments analysis is to use the geometric information of the fiber addresses to determine the general direction of the photon shower. First a set of hits data, like that shown in figure 7, has its average position calculated is the X and Z dimensions. This value is shown in figure 7 as a large diamond in the center of the figure and is referred to as the zero'th order moment. Next this value is used as the origin about which the

average values of the absolute values of X and Z for each fiber hit are calculated. These average values are used to define a direction characterizing the shower direction. This first moment is shown by the thin vertical line passing through the large

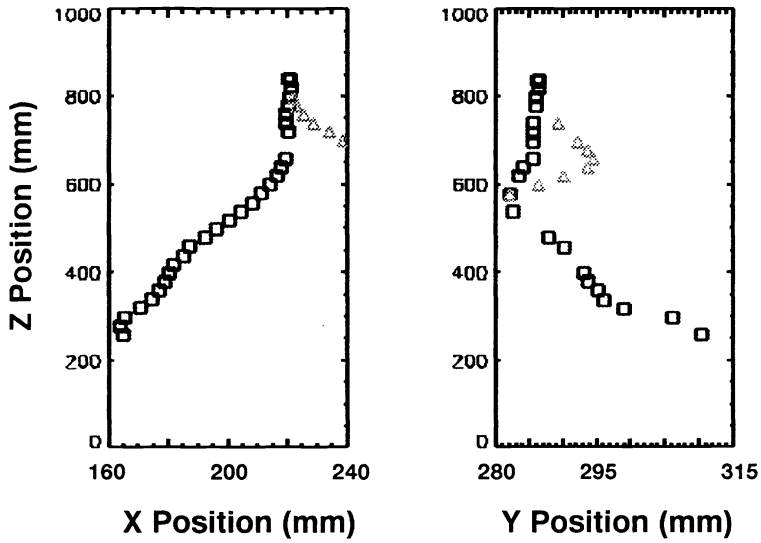


**Figure 8: Reconstructed tracks**

diamond. Next, the hits data are divided in half by a line perpendicular to the first moment passing through the zero'th monent, shown as a thin horizontal line in figure 7. The data are then divided by this line into two sets. The calculation of the zero'th and first moments is repeated for the two separate data sets and these sets are subdivided again as before for a total of four identified data sets. In the case where there are less than 10 fiber hits in the X-Z or Y-Z plane, the iterated analysis is not performed.

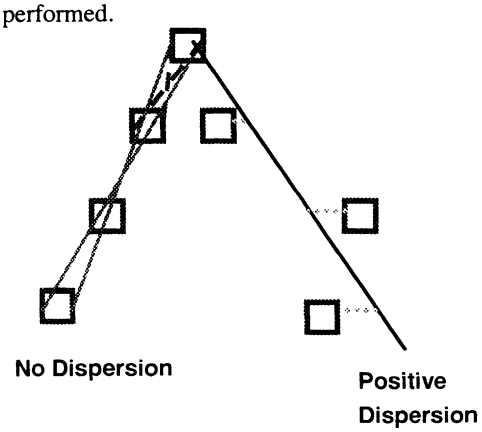


**Figure 9: Diagram of angular reconstruction algorithm**

For each identified subset, several parameters are calculated: the average dispersion of hits about the first moment, the total number of hits in the set, and the average number of hits per plane. Combining these parameters sequentially in one direction and then in the opposite direction for the data subsets produces two scalar values whose difference determines the end of the shower with the conversion vertex. The track reconstruction algorithm then builds candidate photon tracks starting from the identified vertex. A set of reconstructed particle tracks is shown in figure 8. The thicker square at the top is the point identified as the vertex. The squares are fiber hits assigned by the tracker algorithm to one track and the triangles are

hits assigned to a second track. Gaps in the data are visible since the efficiency for minimum ionizing particle detection in these simulations is set at ~90%.

Figure 9 illustrates the two techniques being used to calculate track direction. The left hand track shows a set of points that yield a straight line track with no dispersion, called here a tolerant track. In this case there is a range of angles for which a straight line could be fitted to the track. The right hand track is fit to points were no single straight line can be made to pass through all the points, and is identified as a track fit with positive dispersion. This kind of track fitting is accomplished with a second routine that minimizes the absolute magnitude of the dispersion (shown as the horizontal dotted lines) about the best fit track.

### 3.3 FiberGLAST Response Characteristics

Figures 10 and 11 show the gamma-ray effective area for level-0 triggers compared to that for the worst-case level-1 algorithm, which uses very broad anti-coincidence rejection windows. The "self-veto" effect is apparent at high energies, where the level-1 accept effective area is substantially lower than that of level-0 triggers. Much of this effect is an artifact of the current level-1 algorithm and the situation will improve significantly with an optimized system. However, even with the worst case trigger algorithm, the *FiberGLAST* system exceeds the baseline GLAST performance requirements by maintaining a ~10,000 $cm^2$ effective area above 1 GeV even at large angles.

Figure 12 shows the preliminary estimates of the point spread function at 68% containment for normal incidence photons. The solid line represents the simulation results and the dashed line shows the instrument performance requirements. It should be possible to improve the point spread function at higher energies using more refined techniques than have been applied to the data to date.

The energy resolution for fiberGLAST is calculated using the hit position data of the fiber hits from the tracker and the position and energy deposition data from the hits in the calorimeter. Preliminary normal incidence estimates are shown in figure 13. Below 1Gev, techniques using linear combinations of the tracker and calorimeter hit numbers produce reasonable resolution estimates. Above 1 GeV, the energy deposition pulse height information in the calorimeter must be taken into account. In addition, the data must be adjusted to reflect the differential cascade development. Further studies are underway to develop more effective energy estimation algorithms.

## 4. SUMMARY

The FiberGLAST instrument uses advanced technology to optimize its detector response characteristics for astrophysical observations. Since the readout electronics are distributed around the perimeter of the instrument, the area and number of detector planes that can be practically deployed in the GLAST mission is much larger than what is possible with competing technologies. This design flexibility allows us to tailor the instrument for maximum performance, rather than compromise the design to satisfy power and weight constraints. Since our primary vendors are identifed, and a relatively lean management structure has been adopted, our cost and risk factors can be determined with confidence.

## REFERENCES


1. G. N.Pendleton, R. M. Kippen, R. S. Mallozzi, G. A. Richardson, J. Buckley, M. H. Israel, K. Rielage, G. J. Fishman, T. A. Parnell, M. J. Christl, R. B. Wilson, T. Koshut, "*Scientific capabilites of SIFTER for discovering and monitoring gamma-ray bursts and active galactic nuclei*", Proceedings of SPIE, Hard X-Ray and Gamma-Ray Detector Physics and Applications, Ed. F. Patrick Doty, Richard B. Hoover, Vol. 3446, pp 247-256, SPIE, Bellingham, Wa. 1998

2. Aarnio, P. A., "*FLUKA User's Guide*", technical Report TIS-RP-190, CERN, Geneva, Switzerland, 1990

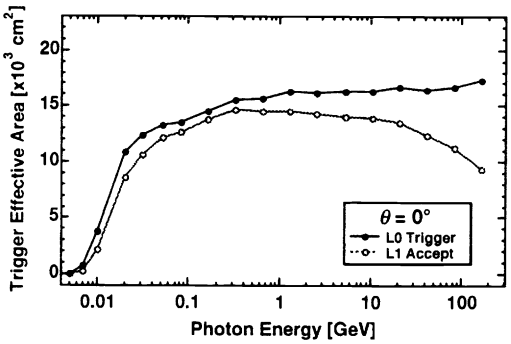


**Figure 10: Normal Incidence Effective Area as a function Photon Energy**

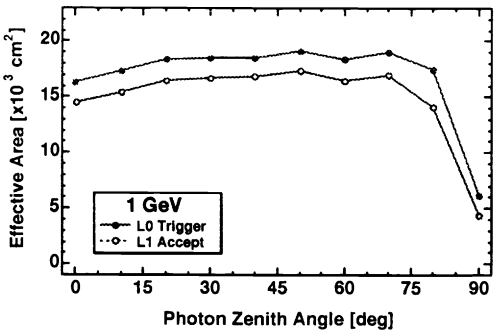


**Figure 11: Effective area as a function of incident photon angle at 1 GeV.**

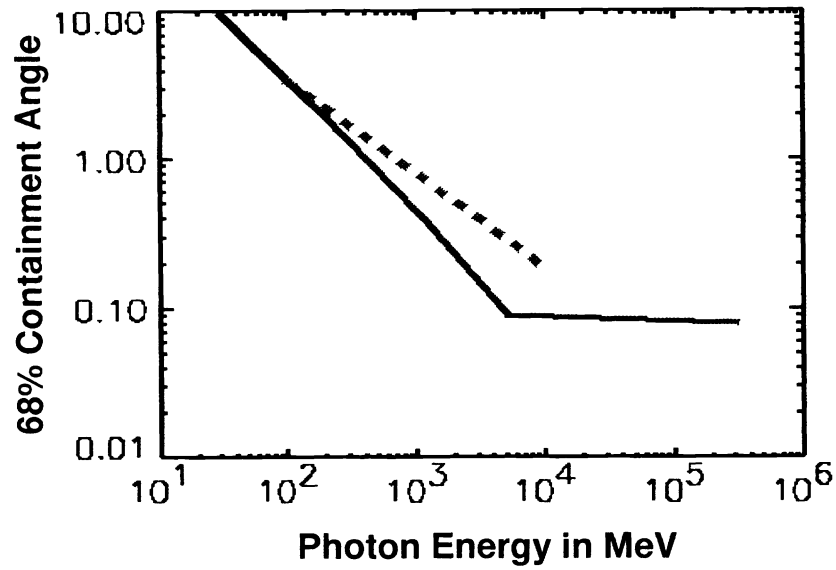


**Figure 12: Normal incidence point spread function as a function of photon energy**

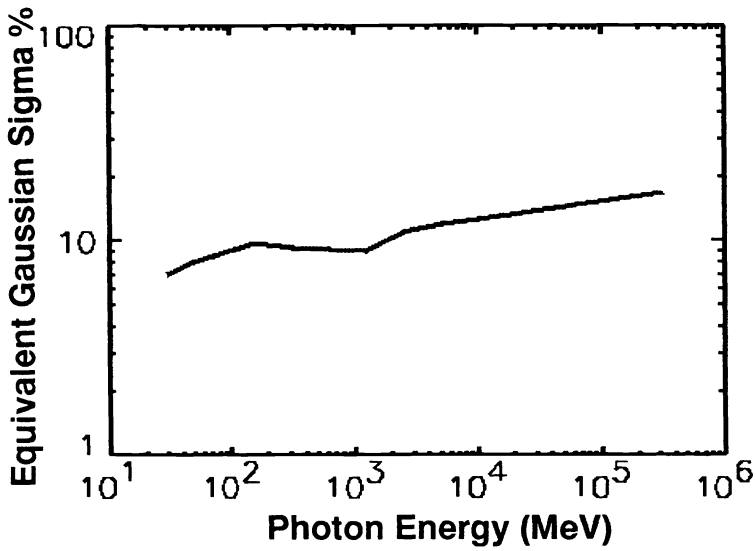


**Figure 13:Normal incidence energy resolution as a function of photon energy**